

Swarm-Based Trajectory Generation and Optimization for Stress-Aligned 3D Printing

XAVIER GUIDETTI^{1,2}, EFE C. BALTA^{1,2}, (Member, IEEE), and JOHN LYGEROS¹, (Fellow, IEEE)

¹Automatic Control Laboratory, ETH Zurich, Physikstrasse 3, 8092, Zurich, Switzerland (e-mail: {xaguidetti,jlygeros}@control.ee.ethz.ch)

²Inspire AG, Technoparkstrasse 1, 8005, Zurich, Switzerland (e-mail: efe.balta@inspire.ch)

Research supported by Innosuisse (project №102.617 IP-ENG) and by the Swiss National Science Foundation under NCCR Automation (grant №180545)

ABSTRACT In this study, we present a novel swarm-based approach for generating optimized stress-aligned trajectories for 3D printing applications. The method utilizes swarming dynamics to simulate the motion of virtual agents along the stress field of a part under loading conditions. The resulting agent trajectories are then used as print trajectories. With this approach, the complex global trajectory generation problem is subdivided into a set of sequential and computationally efficient quadratic programs. Through comprehensive evaluations in both simulation and experiments, we compare our method to state-of-the-art approaches. Our results demonstrate a remarkable improvement in computational efficiency, achieving a $115\times$ faster computation speed than existing methods. This efficiency, combined with the possibility to tune the trajectory spacing to match the deposition process constraints, makes the potential integration of our approach into existing 3D printing processes seamless. Additionally, the open-hole tensile specimen produced on a conventional fused filament fabrication setup with our algorithm achieves a notable $\approx 10\%$ improvement in specific modulus compared to existing trajectory optimization methods.

INDEX TERMS 3D printing, additive manufacturing, fused filament fabrication, stress-aligned printing, swarming, trajectory optimization

I. INTRODUCTION

In 3D printing, a desired three-dimensional part is created by depositing material in a layerwise fashion. This family of manufacturing processes, also known as Additive Manufacturing (AM), enables the creation of complex geometries and has been steadily gaining popularity. The most widely used AM technique is Fused Filament Fabrication (FFF) [1], which is also known as Fused Deposition Modeling (FDM) or Material Extrusion Additive Manufacturing [2]. In FFF, a numerically controlled heated extruder moves along a predefined trajectory while depositing melted plastic, forming the desired 3D geometry. Typically, the geometry to be manufactured is first sliced into equally spaced planes (known as *planar* printing) [3] or two-dimensional manifolds (known as *non-planar* printing) [4]–[6]. The slice is then filled with printing trajectories. This is achieved via a *slicer* software, which focuses on generating trajectories that form the part in a rapid and precise manner. Depending on the used material, desired geometry, printing equipment, and required geometrical accuracy, the slicing and trajectory generation process can be adapted to optimize the properties of the manufactured part [7]–[10].

The recent developments of high-performance materials, paired with technological improvements in the printing process, have enabled the usage of parts produced with FFF in a wide range of applications where high strength and stiffness are required [11], [12]. Motivated by these developments, recent works have focused on generating stress-aligned printing trajectories that maximize the mechanical properties of FFF printed parts, both in the planar [13] and non-planar case [14], [15]. Other works have tackled the same problem for the specific case of fiber-reinforced filaments, which need to be printed in a continuous fashion [16]–[18]. The key idea in this field of research is that, for a given material, manufacturing process, and geometry, there exists a stress-aligned trajectory that produces the desired part while improving its strength and stiffness under a general or specific load case. Finding such trajectories is a challenging task due to complex part features, manufacturing process constraints, and the required geometrical accuracy. The surveyed works that produce acceptable results in practice generally compute print trajectories by solving a very large optimization problem, which is often complex and time-consuming. Additionally, these methods produce a single solution that cannot be tuned or refined to

exactly match the printing process properties and mechanical requirements.

In this work, we propose a novel approach for the generation of stress-aligned print trajectories, based on swarming dynamics. Each computed print line is the trace of a simulated agent moving through the part to be printed. Agents move in a swarm, and their motion is dictated by the stress field generated by the part's load case, producing stress-aligned trajectories. By utilizing a swarm-based approach, the complex stress-aligned trajectory generation problem is broken down into a set of sequential and computationally efficient optimization problems. This significantly reduces the total time required for optimization. Additionally, the swarming dynamics enable great flexibility: our swarm-based trajectory generation method can be fine-tuned to produce trajectories that perfectly satisfy the printing process limitations. The main contributions of this work are:

- A novel, computationally efficient, and flexible swarm-based approach to stress-aligned trajectory generation for 3D printing,
- A study of the proposed method's behavior under different settings, and
- An experimental comparison of swarm-based stress-aligned trajectory generation with a state-of-the-art method.

In Section II we introduce the methods used in our approach and discuss related literature. Section III details the swarm-based trajectory generation method. In Section IV we analyze the performance of our method in detail and benchmark it. Section V concludes the paper.

II. BACKGROUND

A. FINITE ELEMENT ANALYSIS

Finite Element Analysis (FEA) is a well-studied and widely used method to numerically simulate the stress field inside a loaded geometry [19]. We utilize FEA to compute the stress along which the printing trajectories for the optimized part will be aligned. In FEA, the part to be manufactured is first subdivided into a tetrahedral mesh. Then the forces produced by the predefined load case are added to the problem as boundary conditions. After assigning the mechanical properties of the part (i.e. Young's modulus and Poisson ratio), an FEA solver is used to find a numerical solution to the resulting set of differential equations. Solving this discretized problem corresponds to finding a Cauchy stress tensor σ for each node in the mesh. Typically, the Cauchy stress tensor is decomposed using eigenvalue decomposition to obtain the principal stresses (eigenvalues) and principal directions (eigenvectors) [20]. Now, the stress tensor can be represented as a diagonal matrix in a reference frame oriented along the principal directions of the decomposition. The diagonal entries σ_1 , σ_2 and σ_3 of the principal stress matrix are ordered such that $|\sigma_1| \geq |\sigma_2| \geq |\sigma_3|$. In this work, we only consider the principal stress σ_1 and the corresponding normalized eigenvector \hat{s} . This eigenvector indicates the direction along

which the principal stress acts. We indicate the product of the principal stress with the corresponding normalized eigenvector as $s = \sigma_1 \hat{s}$, and we call it the *local principal stress vector*. We denote with $\sigma_{\max} = \max |\sigma_1|$ the largest principal stress across all nodes in the mesh.

B. STRESS-ALIGNED PRINTING

The goal of stress-aligned printing is to optimize the internal structure of a 3D-printed part to enhance its mechanical performance. The approach exploits the anisotropic nature of AM processes like FFF, that produces parts whose mechanical properties are better in the direction in which the plastic filament has been deposited. This effect can be moderate with materials such as PolyLactic Acid (PLA) (see Fig. 2 from [14]) or very pronounced with materials such as Liquid Crystal Polymers (LCP) [21]. After conducting an FEA for a given geometry and load case, the field of local principal stress vectors is used to guide the trajectory generation process to produce trajectories for which the local printing direction is aligned with the local principal stress. This has been shown to maximize the strength and stiffness of the final object under the given load case [3], [6], [14], particularly when variable line width printing is utilized [22], [23].

In earlier works, the stress alignment of trajectories has been achieved at the expense of the computational efficiency and flexibility of the approach. Existing methods require long and complex computations, often relying on commercial optimization solvers, which makes them unsuitable for widespread use in conventional slicers. Furthermore, for a given geometry and load case, a unique trajectory is generated, with no possibility for refinement. This is particularly limiting, since the manufacturability of trajectories is a central issue in FFF. Generally, a stress-aligned trajectory for a complex part is characterized by a variable spacing between the print lines. However, the possibility of depositing lines of variable width is constrained by the material properties and the extrusion process. Attempting to print beyond these constraints necessarily produces over- or under-extrusion, strongly reducing the quality of the printed part and its mechanical properties [24], [25]. Here we address these shortcomings by developing a computationally efficient stress-aligned trajectory generation algorithm that can be tuned to produce trajectories with a desired distribution of line spacing, ensuring manufacturability.

C. SWARMING

Numerous methods for swarm formation, modeling, and navigation for multiple autonomous agents have been proposed in the literature [26]–[28]. Often, the interactions between individuals (or between individuals and the space surrounding them) have been modeled using artificial potential functions. The main applications driving this line of research have been robot navigation and control [29]–[31] or multi-agent coordination [32]. Interestingly, however, the inspiration for a more general approach to the study of swarm aggregation came from mathematical biology [33], [34]. Gazi and Passino

[35]–[37] have introduced a class of attraction and repulsion functions between individuals that ensure the aggregation of a swarm moving through an environment prevent individuals from making contact with each other and allow for formation control. They have further extended their work to follow an energy approach [38]. Here, the total energy of a swarm is given by the sum of its kinetic and potential energies. A swarm's kinetic energy is simply the sum of the kinetic energies of its individual components, as defined in classical mechanics. The notion of the potential energy of a swarm has been extended beyond classical physical potential energy to also include aggregation, environment, and predator potentials. Given these notions, it is possible to model a swarm by applying a Lagrangian approach to the swarm's total energy. Intuitively, the agents of a swarm have a tendency to maintain their kinetic energy and attain minimal potential energy. A flock of birds or a school of fish, for example, seek to travel with constant speed and direction (thus avoiding kinetic energy variations), to maintain a comfortable and safe distance between individuals (minimizing the aggregation potential), to explore areas rich in food (minimizing the environment potential), and to scatter and flee in the presence of threats (minimizing the predator potential).

III. METHOD

The approach we propose originates from the idea that the motion trajectories of a swarm of virtual point-mass agents can be used as manufacturing trajectories. If the swarm is carried through a mechanically loaded part by the load-induced stress flow, the resulting manufacturing trajectories are stress-aligned. As commonly done in the literature [6], [14], we separate the tasks of slicing the part and generating trajectories on a slice. Depending on the application, the generated trajectories can be projected onto non-planar layers following the approaches in [6], or used directly as layerwise print paths in planar printing.

The generation of trajectories for FFF has specific requirements and peculiarities that prevent the direct application of the existing approaches to swarm modeling:

- 1) Agents in the swarm must avoid moving through existing trajectories,
- 2) The set of trajectories must cover the entire part, and
- 3) Agents can be added to or removed from the swarm at will.

Condition 1 is not enforced in classical swarm modeling, since physical agents must simply avoid collisions among each other. Only the present location of agents is relevant for planning, and agents are allowed to cross existing trajectories. In swarming for manufacturing, however, both a spatial and temporal separation must be maintained between agents: the manufacturing trajectories cannot overlap as depositing material twice at the same location creates defects in the part. Condition 2 ensures that the outside of the part produced with the generated trajectories matches the desired geometry and that no voids are left inside the part. Additionally, in FFF (and in AM in general) the rate of material deposition is bounded.

Hence, if trajectories are too far apart the space between them cannot be entirely filled, whereas if trajectories are too close together too much material will be deposited at the same location. Finally, Condition 3 exploits the non-physical nature of agents in the manufacturing problem to simplify the part coverage problem (Condition 2). Unlike physical agents, we can change the number of agents in the swarm at any time. For example, it is possible to *spawn* new agents (which will produce a new manufacturing trajectory) where existing agents diverge, or to *kill* existing agents (which will interrupt an existing manufacturing trajectory) where trajectories compress.

A. SWARM-BASED TRAJECTORY PLANNING FOR MANUFACTURING

Our approach is inspired by the notions of aggregation and environment potentials from [38], which we have adapted to the context of manufacturing. We create a swarm of agents at the location where the largest external force is applied to the part. At initialization, the agents are homogeneously spaced, and neighboring agents are at a predefined distance matching the nominal desired distance between FFF print lines. We define the swarm potential as

$$P = P_a + KP_e, \quad (1)$$

where P_a and P_e are the aggregation and environment potentials of the swarm, and $K > 0$ is a tuning constant. P_a encodes the quality of the swarm formation: it is minimal when the spacing between neighboring agents corresponds to a predefined desired distance and increases in case of spacing deviations. P_e quantifies the stress alignment of the agents' motion: it is minimal when agents follow the stress flow exactly, and increases when they deviate from it. Using this swarm potential, the print trajectories are generated according to Algorithm 1; the details of each step are provided below.

Algorithm 1 Swarm-Based Trajectory Generation

Require: Initial location, step size h , desired distance l , FEA simulation, K

- 1: **while** Part is not fully covered **do**
 - 2: Advance each agent by one step size along the local principal stress direction
 - 3: Reposition agents by minimizing P
 - 4: **if** Two agents are too close together **then**
 - 5: Kill one of them
 - 6: **end if**
 - 7: **if** Two agents are too far apart **then**
 - 8: Spawn one agent in between
 - 9: **end if**
 - 10: **end while**
-

B. STEP DIRECTION AND SIZE

As the principal stress vectors forming the stress flow originate from the eigenvectors of the Cauchy stress tensor, only their direction is relevant to the stress alignment problem,

while their orientation is not. Intuitively, local alignment between a print line and a stress vector is left unchanged by flipping the vector orientation. To produce a stress flow free from this 180° *ambiguity* (i.e. heterogeneous stress vectors orientations), past approaches have used simulated annealing [39] and rectification along the main Cartesian component [6]. Here, we exploit the particle swarming nature of the approach to solve the orientation ambiguity by using the momentum of the agents. At each iteration, an individual agent is displaced according to the local principal stress vector *direction*. However, we select the displacement *orientation* that best aligns with the displacement of the agent in the previous iteration, implicitly preventing sharp changes in an agent's trajectory.

To ensure that agents advance in a uniform front, every agent moves by a predefined and fixed step size; this is done to simplify the optimization problem. To ensure that no trajectories overlap, we set the step size $h = l$, where $l > 0$ is the desired distance between neighboring agents.

We define a slice \mathcal{S} as a compact, connected subset of \mathbb{R}^2 . At iteration k , \mathcal{S} contains $N_k \in \mathbb{N}$ agents. We consider an agent $x_i \in \mathcal{S}$, with $i \in \{1, \dots, N_k\}$. The agent is located at $x_i(k)$ and the local principal stress direction is $\hat{s}(x_i(k))$ (which we project on the slice if necessary). After one step, the agent will be located in

$$t_i(k+1) = x_i(k) + \mu \hat{s}(x_i(k))h. \quad (2)$$

Here we set $\mu = 1$ when $\hat{s}(x_i(k)) \cdot (x_i(k) - x_i(k-1)) \geq 0$ and $\mu = -1$ otherwise, where \cdot denotes the inner product in \mathbb{R}^2 . The forward step motion of two agents is illustrated in Fig. 1.

C. AGENT POTENTIAL FUNCTIONS

The potential functions commonly utilized in the literature [38] are nonlinear, and the resulting total potential of a swarm is generally non-convex. Optimizing such functions remains a complex, inefficient, and time-consuming task [40], [41]. We introduce quadratic environment and aggregation potential functions to simplify and accelerate the potential optimization problems. This makes minimizing Eq. (1) a quadratic programming (QP) problem [42], which can be solved efficiently by existing solvers.

To define the environment potential P_e , let us consider an individual agent $x_i \in \mathcal{S}$ that has advanced by a step in the local stress direction following Eq. (2) and is now located in $t_i(k+1)$. We can imagine that $t_i(k+1)$ is the “ideal” location for the agent, as the trajectory of the agent between $x_i(k)$ and $t_i(k+1)$ is aligned with the local stress vector $\hat{s}(x_i(k))$. We assign the agent a *virtual mass*

$$m_i(k+1) = \frac{|\sigma_1(x_i(k))|}{\sigma_{\max}}, \quad (3)$$

which is proportional to the local stress vector magnitude $\sigma_1(x_i(k))$. We can now imagine the environment potential associated to the agent as the *energy* required to reposition

the agent away from its ideal location $t_i(k+1)$, and bring it to a final location $x_i(k+1)$, as shown in Fig. 1. We define

$$p_e(x_i(k+1)) = m_i(k+1) \|x_i(k+1) - t_i(k+1)\|_2^2, \quad (4)$$

which is a quadratic function with a global minimum $p_e(x_i(k+1)) = 0$ when the agent is not repositioned. Using the virtual mass term m , we make the repositioning of agents with a larger associated stress more costly. This ensures that the alignment between trajectories and stress will be higher where the local stress is larger.

The aggregation potential P_a is computed by comparing the locations of neighboring agents to avoid agent trajectories that overlap or cross. An intuitive way to achieve this would be to encode existing trajectories as locations to be avoided by the moving agents (for example, by including them in the environment potential). However, this approach presents a major scalability issue. As the number of iterations of Algorithm 1 grows, the size of existing trajectories keeps on increasing, making the size and complexity of the optimization problem larger and larger, and leading to computation issues. The scalability problem is amplified if the parts to be manufactured are large with respect to agent spacing. We avoid this issue by using potential functions that only depend on the location of other agents at the *current* iteration, and not at *all past* iterations. Instead of evaluating the distance between agents in a straight line, we decompose it into *radial distance*, which is measured perpendicularly to the displacement direction of the agents, and *axial distance*, measured in the displacement direction of the agents. We achieve an orderly advance of the agents by keeping neighboring agents at a desired radial distance and by minimizing their axial distance. Thus, the swarm advances as a front of homogeneously spaced agents, which are roughly aligned along a front line. We consider two agents $x_i, x_j \in \mathcal{S}$, with $i, j \in \{1, \dots, N_k\}$ and $i \neq j$. Their locations at iteration $k+1$ are denoted as $x_i(k+1)$ and $x_j(k+1)$. We define the vectors

$$\mathbf{v} = x_j(k+1) - x_i(k+1), \quad (5)$$

corresponding to the directed distance between the agents, and

$$\mathbf{d} = -(x_i(k) - x_i(k-1) + x_j(k) - x_j(k-1))^\perp, \quad (6)$$

$$\hat{\mathbf{d}} = \frac{\mathbf{d}}{\|\mathbf{d}\|_2}, \quad (7)$$

the unit vector orthogonal¹ to the averaged direction of travel of the two agents in the previous iteration. Both vectors are shown in Fig. 1 for clarity. We define the aggregation potential p_a of agent x_i with respect to its neighbor x_j as

$$p_a(x_i(k+1)|x_j) = (\|proj_{\hat{\mathbf{d}}} \mathbf{v}\|_2 - l)^2 + \|oproj_{\hat{\mathbf{d}}} \mathbf{v}\|_2^2, \quad (8)$$

where the norm in the first term, encoding the requirement to keep the radial distance close to the desired distance l , is computed as

$$\|proj_{\hat{\mathbf{d}}} \mathbf{v}\|_2 = \mathbf{v} \cdot \hat{\mathbf{d}}, \quad (9)$$

¹The notation \cdot^\perp used in Eq. (6) corresponds, in two dimensions, to a counterclockwise rotation of the vector by 90°, i.e. $\mathbf{a}^\perp = \begin{bmatrix} 0 & -1 \\ 1 & 0 \end{bmatrix} \mathbf{a}$.

and the norm in the second term, used to minimize the axial distance, is computed as

$$\| \text{proj}_{\hat{\mathbf{d}}} \mathbf{v} \|_2 = \| \mathbf{v} - (\mathbf{v} \cdot \hat{\mathbf{d}}) \hat{\mathbf{d}} \|_2. \quad (10)$$

As $\hat{\mathbf{d}}$ and l are fixed, p_a is a quadratic function depending on $x_i(k+1)$ and $x_j(k+1)$, and has a global minimum $p_a(x_i(k+1)|_{x_j}) = 0$ when the two agents advance side by side at distance l .

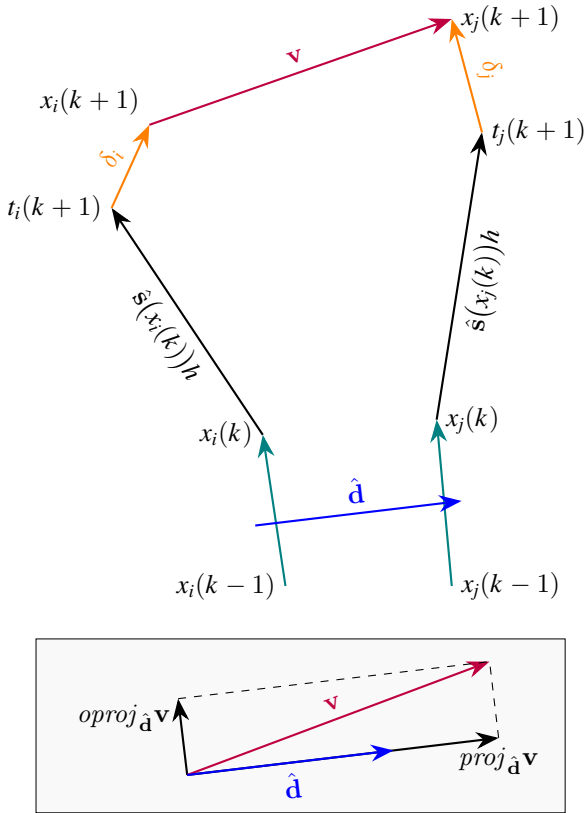


FIGURE 1. Notation of the agent locations and distance vectors utilized in the definition of the environment potential p_e and of the aggregation potential p_a . Two agents located in $x_i(k)$ and $x_j(k)$ follow the respective local stress vectors $\mathbf{s}(x_i(k))$ and $\mathbf{s}(x_j(k))$ and advance by one step size h to $t_i(k+1)$ and $t_j(k+1)$. Vectors \mathbf{d}_i and \mathbf{d}_j are used to compute p_e according to Eq. (4); vectors \mathbf{v} and $\hat{\mathbf{d}}$ used to compute p_a according to Eq. (8). Solving Eq. (13) moves the agents to their optimized locations $x_i(k+1)$ and $x_j(k+1)$.

We greatly simplify the computation task by only comparing *neighboring* agents. Every agent has two neighbors, each being the closest agent in either orientation along the *radial* direction. In simpler terms, agent x_i has neighbors x_{i-1} and x_{i+1} ; any other agent in the swarm has no aggregation potential with respect to x_i . The adjacency of agents is fixed since initialization and does not change during their motion through the part. Given the commutative nature of p_a as defined in Eq. (8), for each pair of adjacent agents x_i and x_{i+1} we add to the computations only the term $p_a(x_i|_{x_{i+1}})$. All other pairs of agents produce $p_a(x_i|_{x_j \neq i+1}) = 0$.

D. BOUNDARY CONDITIONS

By simply defining a swarm of initial agents and making it propagate through the part as explained in Algorithm 1, complete coverage of the part is not guaranteed. In particular, without further constraints, agents are free to step outside the part or to leave an empty space between the part boundaries and the swarm. To avoid such scenarios, we introduce *boundary conditions* to constrain and condition the swarm.

As the swarm is initialized, at the beginning of Algorithm 1, two *boundary agents* are added at the extremities of the swarm. At iteration $k = 0$ we denote the initial swarm $\mathcal{X}(0)$; it is composed of N_0 agents $x_i(0) \in \mathcal{S}$, $i = 1, \dots, N_0$. We create the boundary agents $x_0(0)$ and $x_{N_0+1}(0)$, as shown in Fig. 2. The motion of these two agents is constrained to follow the part boundary. This is ensured by projecting their position on the boundary after they advance, and by allowing them to move only along the boundary trace when they are repositioned. As a consequence, when computing the swarm trajectories, the agents x_i and x_N maintain approximately a distance l from the part boundaries, ensuring complete coverage and avoiding boundary crossings.

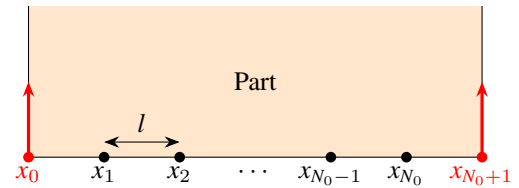


FIGURE 2. Initial swarm of equally spaced agents $x_1(0), \dots, x_{N_0}(0)$ and boundary agents $x_0(0)$ and $x_{N_0+1}(0)$. The displacement of the boundary agents is one dimensional, as they are constrained to follow the part boundary.

During trajectory generation, the swarm of agents can encounter other part boundaries, such as holes. In this case, two additional *internal boundary agents* are added to the swarm in between the two agents closest to the boundary, as shown in Fig. 3. The agents adjacency is updated accordingly, and the trajectory generation according to Algorithm 1 continues. Should the two internal boundary agents meet along their motion (for example, when the swarm has moved past a hole), they are removed from the swarm.

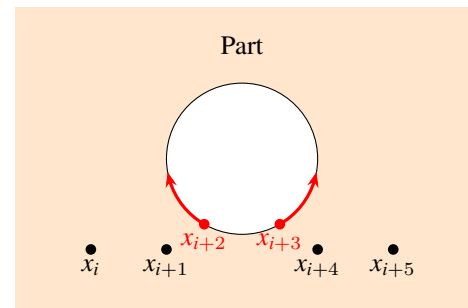


FIGURE 3. Internal boundary agents $x_{i+2}(k)$ and $x_{i+3}(k)$ added to the swarm when encountering a hole in the part

E. OPTIMIZATION PROBLEM

To compute the total potential of the swarm P , which we intend to minimize at each iteration, we first need to define the total environment and aggregation potentials of the swarm. Considering a swarm of N_k agents and boundary agents $x_i(k+1)$, $i = 0, \dots, N_k + 1$, which at iteration $k+1$ we denote $\mathcal{X}(k+1)$, the swarm environment potential is simply

$$P_e(\mathcal{X}(k+1)) = \sum_{i=1}^{N_k} p_e(x_i(k+1)), \quad (11)$$

where the environment potential of an individual agent is given in Eq. (4). Similarly, we define the swarm aggregation potential as

$$P_a(\mathcal{X}(k+1)) = \sum_{i=0}^{N_k} p_a(x_i(k+1)|_{x_{i+1}}), \quad (12)$$

where the aggregation potential of an individual agent is given in Eq. (8) and includes the notion of adjacency.

For a given tuning hyperparameter K , we can formulate the optimization problem being solved at each iteration of Algorithm 1 as

$$\mathcal{P}(\mathcal{X}(k+1)) = \min_{\mathcal{X} \in \mathcal{X}} P_a(\mathcal{X}(k+1)) + KP_e(\mathcal{X}(k+1)) \quad (13)$$

$$\begin{aligned} \text{s.t.} \quad & \|proj_{\hat{s}(x_i(k))} \delta_i(k+1)\|_2 \leq h/4 \quad i = 1, \dots, N_k \\ & \|opproj_{\hat{s}(x_i(k))} \delta_i(k+1)\|_2 \leq h/8 \quad i = 1, \dots, N_k \\ & x_i(k+1) \in \partial S \quad \text{for boundary agents,} \end{aligned}$$

where $\delta_i(k+1) = (x_i(k+1) - t_i(k+1))$. The definitions of the projection terms in the constraints correspond to those given in Eq. (9) and Eq. (10), and ∂S indicates the boundary of the slice. The inequality constraints limit the displacement of agents to a box around their ideal location $t_i(k+1)$, as shown in Fig. 4, and are necessary to ensure that agents keep advancing and do not cross. These constraints are dictated by the nature of the algorithm and are not subject to tuning. With a suitable change of coordinates, all constraints can be transformed into input bounds in the form $a_i \leq x_i(k+1) \leq b_i$. The resulting problem is a box-constrained QP, which can be solved very efficiently.

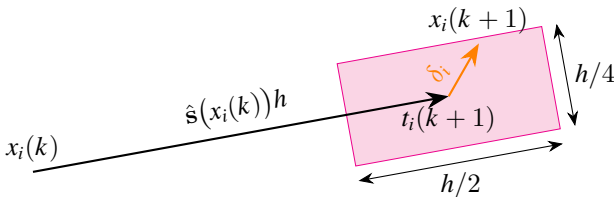


FIGURE 4. Representation of the constraints used in the optimization problem (13) to limit the displacement of the agents around their ideal location $t_i(k+1)$. The two constraints form the box depicted in magenta, which constrains $x_i(k+1)$.

F. KILLING AND SPAWNING

At every iteration of Algorithm 1, we study the swarm (which we denote in this section with $\mathcal{X}_0(k+1)$) to identify the agent with the closest neighbor and the agent with the furthest neighbor. This corresponds to locating the regions where the trajectories are most compressed and most expanded. In the first case, we kill the *compressed* agent to form the swarm $\mathcal{X}_{-1}(k+1)$; in the second case, we spawn a new agent in the empty space between neighbors to form the swarm $\mathcal{X}_{+1}(k+1)$. We then solve the optimization problem (13) for the three configurations to obtain the optimal values $\mathcal{P}(\mathcal{X}_0(k+1))$, $\mathcal{P}(\mathcal{X}_{+1}(k+1))$, and $\mathcal{P}(\mathcal{X}_{-1}(k+1))$. Finally, after normalizing the optimized potential of each swarm with the number of agents it contains, we can make a comparison. We select and keep for the next iteration the swarm

$$\mathcal{X}(k+1) = \arg \min_{q=-1,0,1} \frac{\mathcal{P}(\mathcal{X}_q(k+1))}{N_k + q}, \quad (14)$$

which has the lowest potential among the evaluated scenarios. This approach relies on heuristics which make only one spawning or one killing possible at each iteration. This choice was made to reduce the computational burden, as it allows Algorithm 1 to change the number of agents in the swarm in a principled way, while only solving Eq. (13) three times per iteration.

IV. RESULTS

In this section, we test and benchmark the swarm-based trajectory generation algorithm on a demonstrator part. The part we selected is a loaded open-hole tensile specimen. The specimen is taken from the ASTM standard for open-hole tensile strength of polymer matrix composite laminates [43], and described in Fig. 5. We first analyze the behavior of Algorithm 1 by studying the trajectories generated for the specimen. Then, we conduct an experiment to quantify the improvements obtained in the specimen strength via the proposed method.

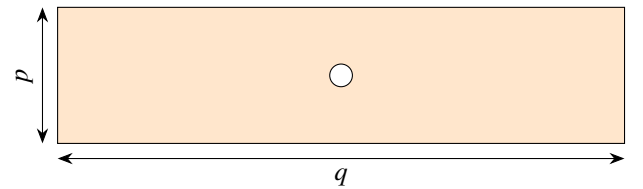


FIGURE 5. Open-hole tensile specimen according to [43]. The dimensions are $p = 36$ mm and $q = 150$ mm, and the thickness is 2 mm. The hole has a diameter of 6 mm. The specimen is evaluated in a tensile strength test, with tension applied at the two narrow extremities.

A. TRAJECTORY GENERATION

We implement the swarm-based trajectory generation algorithm in Python (including SciPy [44] and NumPy [45]); the optimization problems are solved efficiently by utilizing CasADi [46] as an interface and OSQP [47] as a solver. We

first discuss the effect of the hyperparameter K and then compare the trajectory generation performance with the method from [6].

In Eq. (13), K modifies the relative weight of the aggregation potential P_a with respect to the environment potential P_e . Selecting smaller values of K in the optimization produces swarms that mostly minimize P_e : this corresponds to better swarming behavior (i.e. agents advancing as a front and evenly spaced) at the expense of stress alignment. Conversely, larger values of K increase the importance of P_a in the optimization problem: the agents follow the stress in the part more, but the swarming behavior is worsened.

Suitable values of K are geometry and load dependent, and can be found numerically. For example, in Fig. 6 we show the trajectories generated around the hole of the tensile specimen for three different values of K . With $K = 0.5$ (Fig. 6a) the trajectories are uniformly spaced, but they follow the stress circulating around the hole poorly, which reduces the manufactured part strength. With $K = 50$ (Fig. 6c) the trajectories follow the stress around the hole, but become very compressed in the regions to its left and right, which can cause defects in the manufacturing process. The intermediate case, produced with $K = 5$ (Fig. 6b) results in a satisfactory trade-off, with the trajectories showing a better stress-following behavior than in the $K = 0.5$ case, and a better swarming behavior than in the $K = 50$ case.

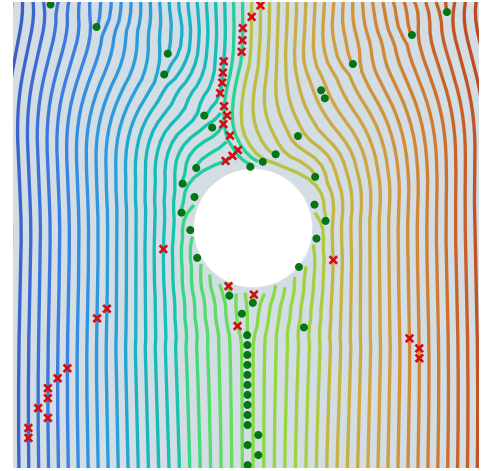
To quantify the effect of K , we analyze stress alignment and trajectory spacing. For stress alignment, we propose the metric

$$\bar{\beta} = \frac{\sum_{z=1}^Z m_z \|\hat{\mathbf{s}}_z \cdot \mathbf{p}_z\|}{\sum_{z=1}^Z m_z}, \quad (15)$$

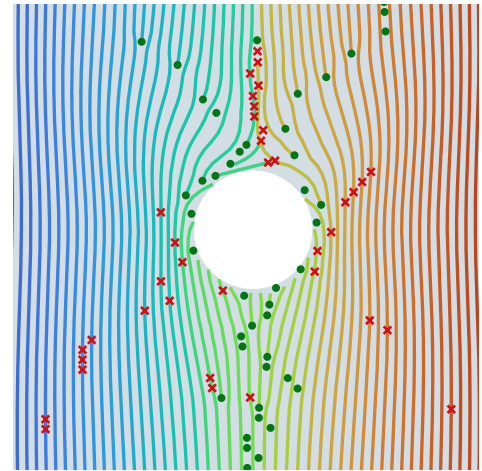
where z indexes all the Z points in a set of generated trajectories, and $\hat{\mathbf{s}}_z$ and \mathbf{p}_z are the normalized local stress and the printing direction at the point z . The alignment metric $\bar{\beta}$ is weighted by the magnitude of the local stress (encoded in the virtual mass m_z , see Section III-C), and can range between 0 (no alignment) and 1 (perfect alignment). The alignment values for the three studied cases are given in Table 1. For trajectory spacing, we compute the distance of every point in the trajectory set from the following trajectory, and visualize the results as a distribution in Fig. 7. We also compute the variance of each distribution and report it in Table 1. Both metrics are in agreement with the qualitative intuitions obtained from Fig. 6, as both $\bar{\beta}$ and the variance of the distance distribution increase monotonically with K .

We compare Algorithm 1 with the method proposed in [6], a state-of-the-art method for stress-aligned trajectory generation for 3D printing, which we call *global trajectory generation*. We utilize both algorithms to generate print trajectories for one slice of the open-hole tensile specimen detailed in Fig. 5, with a nominal line spacing $l = 0.4$ mm.

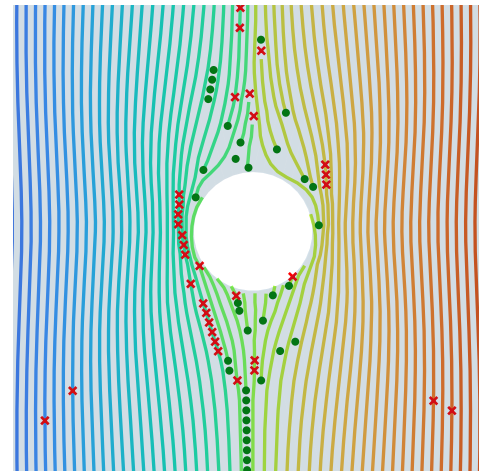
Both algorithms are executed on the same machine, a Windows computer with an Intel Core i9-9900K CPU running at 3.60 GHz and using 48 GB of RAM. The global trajectory generation algorithm solves a single large optimization prob-



(a) $K = 0.5$



(b) $K = 5$

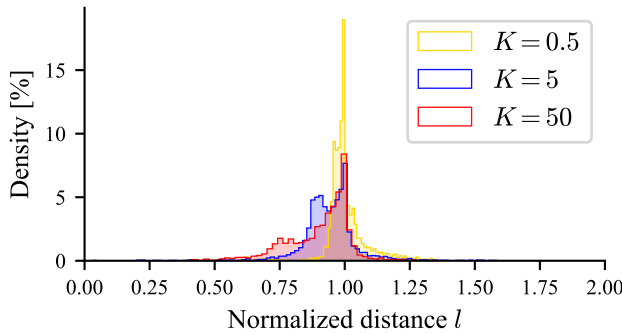


(c) $K = 50$

FIGURE 6. Comparison of manufacturing trajectories for the open-hole tensile specimen generated with different values of the hyperparameter K . The swarm advances from the bottom of the figures towards the top. Green circles and red crosses indicate the locations in which Algorithm 1 evaluates a potential spawn or kill, respectively (see Section III-F).

TABLE 1. Stress alignment and variance of the distribution of distances of the swarm-based trajectory generation method (for different values of K) and of the global trajectory generation method from [6]

	Swarm-based method			Global method from [6]
	$K = 0.5$	$K = 5$	$K = 50$	
$\bar{\beta}$	0.981	0.993	0.998	0.983
Variance	6.1×10^{-3}	12.9×10^{-3}	16.4×10^{-3}	4.4×10^{-4}

**FIGURE 7.** Distribution of distances between trajectories for different values of K . The distance has been normalized using the nominal line spacing $l = 0.4$ mm.

lem and requires 22.7 s to produce the print trajectories. The proposed swarm-based trajectory generation algorithm solves iteratively a large number of simpler optimization problems and completes the task in 198 ms. Thanks to its speed, our approach can be smoothly integrated into existing slicers without affecting user experience.

The 99% reduction in computation time is just one advantage of the method we propose in this work. As discussed by the authors in [6], the global trajectory generation method returns only one solution for a given part and load case, producing trajectories at a fixed (and quasi-constant) distance. This is well suited to printing processes where the deposited line width cannot be changed, but penalizes stress alignment. The trajectories produced with the global method (also reported in Table 1) have $\bar{\beta} = 0.983$ and variance of normalized distances of 4.4×10^{-4} . The trajectory spacing is extremely uniform, and the stress alignment is comparable with the results of Algorithm 1 with $K = 0.5$. When variable line width printing is possible, the swarm-based trajectory generation method offers more flexibility, as trajectories can be adapted by selecting the correct value of K . Allowing a certain amount of variation in the trajectory spacing increases stress alignment (as shown in Table 1) and as a consequence improves the mechanical properties of the part. The tuning of K is however limited by the hardware effectiveness in variable width printing. The stress alignment and trajectory spacing metrics we have proposed are useful tools for choosing the most suitable value of K in practice. Based on these metrics, the ideal K can be found with sampling-based methods, such as random sampling, grid search, or Bayesian optimization.

B. PRINTED PARTS

We manufacture and test, according to [43], open-hole tensile specimens using utilized trajectories generated with:

- 1) A commercial slicer [48] set to *cross-hatching* infill. This infill creates a rectilinear grid by printing one layer as parallel lines in one direction, the next layer rotated by 90° , etc. The direction of the lines is set to 45° with respect to the sides of the specimen. Lines are generated at a distance of 0.4 mm and with a 100% infill. This case constitutes a baseline for non-stress-aligned printing.
- 2) A commercial slicer [48] set to *aligned rectilinear* infill. All lines in the part are parallel and aligned in the direction of the long side of the specimen. Lines are generated at a distance of 0.4 mm and with a 100% infill. This case constitutes a baseline for naive stress-aligned printing.
- 3) The global trajectory generation method from [6]. The nominal line distance is set to 0.4 mm. This case is a state-of-the-art benchmark.
- 4) The proposed swarm-based trajectory generation method with $K = 5$ and a nominal line distance of 0.4 mm. These print trajectories are shown in Fig. 8.

We manufacture three samples for each trajectory generation case. All parts are printed in PLA on a Prusa i3 MK3S machine at a nozzle temperature of 205°C , a bed temperature of 60°C and feed rate of 3150 mm min^{-1} . Samples are tested on a Galdabini Quasar 10 testing machine following [43]. Pictures of the correctly broken samples are shown in Fig. 9. As different trajectory generation methods produce different line spacing distributions, and as this affects the deposition process, the samples have different densities. To make the results comparable, we divide the force measurements by the density of each sample to produce specific stress, specific modulus, and specific strength (which are the density-adjusted equivalents of stress, Young's modulus, and ultimate tensile strength). The results are reported in Fig. 10 and Table 2.

Cross-hatching, the most common trajectory generation technique in FFF, produces the worst performance, with the lowest specific modulus and strength. The aligned rectilinear approach and the global trajectory generation method have a very similar stress-strain curve and a comparable specific modulus. The samples manufactured with our swarm-based trajectories outperform all other samples on the entire strain range. They produce a $\approx 10\%$ improvement in specific modulus compared to the aligned rectilinear and the global methods, while retaining the specific strength of the aligned

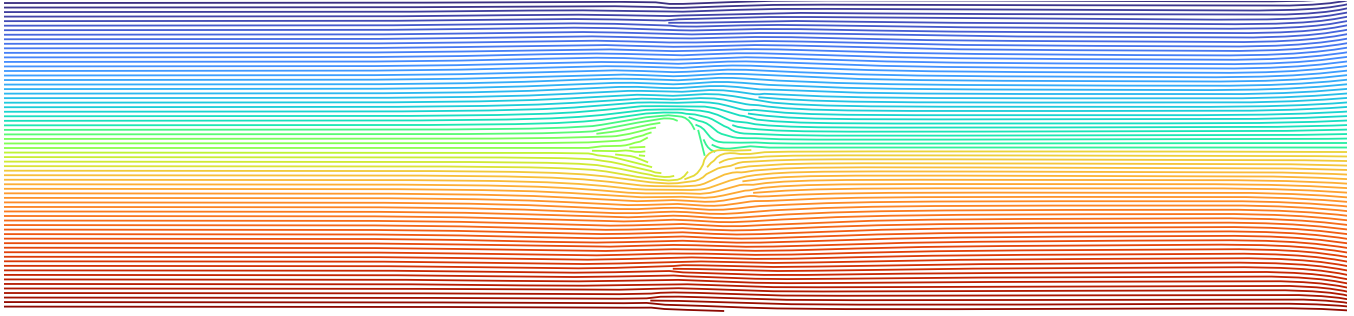


FIGURE 8. Print trajectories for the open-hole tensile specimen obtained with swarm-based trajectory generation (Algorithm 1) and $K = 5$ (corresponding to Fig. 6b). Agents move from the left to the right of the figure.

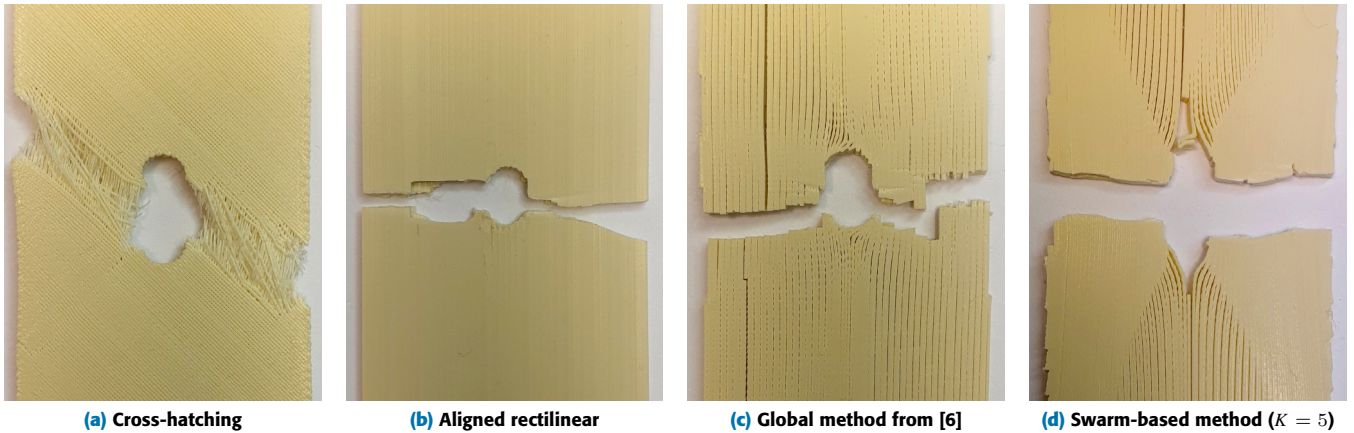


FIGURE 9. Open-hole tensile specimens after a correct failure during testing

TABLE 2. Specific modulus and specific strength of the 12 tested open-hole tensile specimens. The mean values were obtained by averaging the results from each three samples produced with the same trajectory generation method. The uncertainties indicate the range in which the three repetitions lie and help quantify the repeatability error.

	Cross-hatching	Aligned rectilinear	Global method from [6]	Swarm-based method ($K = 5$)
Specific modulus [$\text{Pa kg}^{-1} \text{m}^3$]	$17.48^{+1.62}_{-0.93}$	$19.53^{+0.56}_{-0.61}$	$19.91^{+0.13}_{-0.08}$	$21.73^{+0.18}_{-0.17}$
Specific strength [$\text{Pa kg}^{-1} \text{m}^3$]	$24.57^{+2.38}_{-2.38}$	$44.14^{+0.31}_{-0.44}$	$41.08^{+1.10}_{-0.55}$	$44.07^{+0.14}_{-0.15}$

rectilinear method. Contrarily to previous works [6], [14], this improvement was achieved on a conventional planar printer, using a ubiquitous feedstock material. These results indicate that any combination of commercially available slicers and printers can benefit from our approach to produce stiffer and stronger parts via optimized trajectory generation.

We point out that the high specific strength of the naive aligned rectilinear approach, which lies in the repeatability range of our swarm-based approach, is in all likelihood the consequence of line spacing homogeneity, which enables high-quality deposition on the printer setup. We expect that the constant developments in the field of variable width FFF will reduce the number of deposition defects in the optimized parts, further increasing their strength in practice. Further-

more, the aligned rectilinear approach can be used exclusively in very simple geometries where the load is rectilinear and stress alignment can be achieved intuitively. Conversely, rigorous trajectory optimization methods we develop in our work can be applied to geometries and load cases of any complexity, as was demonstrated in [6].

V. CONCLUSION

In this work, we introduce a novel swarm-based approach to the generation of optimized stress-aligned print trajectories for 3D printing. We evaluate our method and compare it with state-of-the-art approaches, both in simulation and in experiments, focusing on the implications of stress-aligned trajectories for mechanical properties and printing quality. Our re-

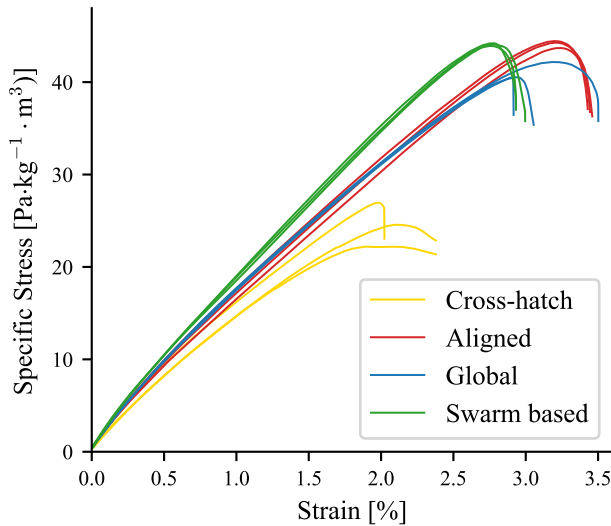


FIGURE 10. Specific stress-strain curve of the 12 tested open-hole tensile specimens

sults demonstrate a significant improvement in computational efficiency with our proposed algorithm, achieving a remarkable $115\times$ increase in computation performance compared to the state-of-the-art method. This computational advantage, coupled with the flexibility of adapting trajectory spacing through hyperparameter tuning, positions our approach as a highly practical solution for seamless integration into existing slicers without compromising user experience. Furthermore, our method allows for enhanced stress alignment, leading to improved mechanical properties of printed parts. The specific modulus of parts produced using our swarm-based trajectories exhibit a $\approx 10\%$ enhancement compared to existing methods. Our findings highlight the potential of trajectory optimization in advancing the mechanical performance and efficiency of 3D printing processes in general and of the prevalent planar FFF of PLA in particular. In future research, we plan to extend the swarm-based approach to the non-planar slicing problem and to solve the slicing and trajectory generation tasks in a single optimization.

ACKNOWLEDGMENT

We gratefully acknowledge the support of NematX AG which has provided the equipment to manufacture the samples.

REFERENCES

- [1] "The state of 3D printing report: 2022 by Sculpteo," <https://www.sculpteo.com/en/ebooks/state-of-3d-printing-report-2022/>, 2022, (Accessed on 01/04/2024).
- [2] ISO/ASTM International, "Additive manufacturing — general principles — fundamentals and vocabulary," International Organization for Standardization, Standard ISO/ASTM 52900:2021, Nov. 2021.
- [3] I. Gibson, D. Rosen, B. Stucker, M. Khorasani, D. Rosen, B. Stucker, and M. Khorasani, *Additive manufacturing technologies*. Springer, 2021, vol. 17.
- [4] G. A. Nisja, A. Cao, and C. Gao, "Short review of nonplanar fused deposition modeling printing," *Material Design & Processing Communications*, vol. 3, no. 4, p. e221, 2021.

- [5] D. Ahlers, F. Wasserfall, N. Hendrich, and J. Zhang, "3D printing of nonplanar layers for smooth surface generation," in *2019 IEEE 15th international conference on automation science and engineering (CASE)*. IEEE, 2019, pp. 1737–1743.
- [6] X. Guidetti, E. C. Balta, Y. Nagel, H. Yin, A. Rupenyan, and J. Lygeros, "Stress flow guided non-planar print trajectory optimization for additive manufacturing of anisotropic polymers," *Additive Manufacturing*, vol. 72, p. 103628, 2023.
- [7] M. J. Hooshmand, S. Mansour, and A. Dehghanian, "Optimization of build orientation in FFF using response surface methodology and posterior-based method," *Rapid Prototyping Journal*, vol. 27, no. 5, pp. 967–994, 2021.
- [8] L. Di Angelo, P. Di Stefano, A. Dolatzehadsomarin, E. Guardiani, and E. Khorram, "A reliable build orientation optimization method in additive manufacturing: The application to FDM technology," *The International Journal of Advanced Manufacturing Technology*, vol. 108, no. 1, pp. 263–276, 2020.
- [9] P. Delfs, M. Tows, and H.-J. Schmid, "Optimized build orientation of additive manufactured parts for improved surface quality and build time," *Additive Manufacturing*, vol. 12, pp. 314–320, 2016.
- [10] C. Wang and X. Qian, "Simultaneous optimization of build orientation and topology for additive manufacturing," *Additive Manufacturing*, vol. 34, p. 101246, 2020.
- [11] B. Brenken, E. Barocio, A. Favaloro, V. Kunc, and R. B. Pipes, "Fused filament fabrication of fiber-reinforced polymers: A review," *Additive Manufacturing*, vol. 21, pp. 1–16, 2018.
- [12] D. Jiang and D. E. Smith, "Anisotropic mechanical properties of oriented carbon fiber filled polymer composites produced with fused filament fabrication," *Additive Manufacturing*, vol. 18, pp. 84–94, 2017.
- [13] L. Xia, S. Lin, and G. Ma, "Stress-based tool-path planning methodology for fused filament fabrication," *Additive Manufacturing*, vol. 32, p. 101020, 2020.
- [14] G. Fang, T. Zhang, S. Zhong, X. Chen, Z. Zhong, and C. C. Wang, "Reinforced FDM: Multi-axis filament alignment with controlled anisotropic strength," *ACM Transactions on Graphics (TOG)*, vol. 39, no. 6, pp. 1–15, 2020.
- [15] X. Guidetti, A. Rupenyan, L. Fassl, M. Nabavi, and J. Lygeros, "Advanced manufacturing configuration by sample-efficient batch bayesian optimization," *IEEE Robotics and Automation Letters*, vol. 7, no. 4, pp. 11 886–11 893, 2022.
- [16] K. Barton, S. Kapila, and L. Y. L. Tse, "Fiber-reinforced 3D printing," Sep. 10 2019, uS Patent 10,406,750.
- [17] X. Chen, G. Fang, W.-H. Liao, and C. C. Wang, "Field-based toolpath generation for 3D printing continuous fibre reinforced thermoplastic composites," *Additive Manufacturing*, vol. 49, p. 102470, 2022.
- [18] Y. Yao, Y. Zhang, M. Aburaia, and M. Lackner, "3D printing of objects with continuous spatial paths by a multi-axis robotic FFF platform," *Applied Sciences*, vol. 11, no. 11, p. 4825, 2021.
- [19] J. N. Reddy, *Introduction to the finite element method*. McGraw-Hill Education, 2019.
- [20] A. F. Bower, *Applied mechanics of solids*. CRC press, 2009.
- [21] S. Gantenbein, K. Masania, W. Woigk, J. P. Sesseg, T. A. Tervoort, and A. R. Studart, "Three-dimensional printing of hierarchical liquid-crystal-polymer structures," *Nature*, vol. 561, no. 7722, pp. 226–230, 2018.
- [22] X. Guidetti, A. Mukne, M. Rueppel, Y. Nagel, E. C. Balta, and J. Lygeros, "Data-driven extrusion force control tuning for 3D printing," *arXiv preprint arXiv:2403.16470*, 2024.
- [23] X. Guidetti, N. Mingard, R. Cruz-Oliver, Y. Nagel, M. Rueppel, A. Rupenyan, E. C. Balta, and J. Lygeros, "Force controlled printing for material extrusion additive manufacturing," *arXiv preprint arXiv:2403.16042*, 2024.
- [24] X. Guidetti, M. Kühne, Y. Nagel, E. C. Balta, A. Rupenyan, and J. Lygeros, "Data-driven process optimization of fused filament fabrication based on in situ measurements," *arXiv preprint arXiv:2210.15239*, 2022.
- [25] G. Siqueira, D. Kokkinis, R. Libanori, M. K. Hausmann, A. S. Gladman, A. Neels, P. Tingaut, T. Zimmermann, J. A. Lewis, and A. R. Studart, "Cellulose nanocrystal inks for 3D printing of textured cellular architectures," *Advanced Functional Materials*, vol. 27, no. 12, p. 1604619, Feb. 2017.
- [26] M. Brambilla, E. Ferrante, M. Birattari, and M. Dorigo, "Swarm robotics: a review from the swarm engineering perspective," *Swarm Intelligence*, vol. 7, pp. 1–41, 2013.
- [27] L. Bayındır, "A review of swarm robotics tasks," *Neurocomputing*, vol. 172, pp. 292–321, 2016.

- [28] S.-J. Chung, A. A. Paranjape, P. Dames, S. Shen, and V. Kumar, "A survey on aerial swarm robotics," *IEEE Transactions on Robotics*, vol. 34, no. 4, pp. 837–855, 2018.
- [29] O. Khatib, "Real-time obstacle avoidance for manipulators and mobile robots," *The international journal of robotics research*, vol. 5, no. 1, pp. 90–98, 1986.
- [30] E. Rimon, *Exact robot navigation using artificial potential functions*. Yale University, 1990.
- [31] E. Rimon and D. E. Kodischek, "Exact robot navigation using artificial potential functions," *IEEE Transactions on Robotics and Automation*, vol. 8, no. 5, pp. 501–518, 1992.
- [32] J. H. Reif and H. Wang, "Social potential fields: A distributed behavioral control for autonomous robots," *Robotics and Autonomous Systems*, vol. 27, no. 3, pp. 171–194, 1999.
- [33] K. Warburton and J. Lazarus, "Tendency-distance models of social cohesion in animal groups," *Journal of theoretical biology*, vol. 150, no. 4, pp. 473–488, 1991.
- [34] D. Grünbaum and A. Okubo, "Modelling social animal aggregations," in *Frontiers in mathematical biology*. Springer, 1994, pp. 296–325.
- [35] V. Gazi and K. M. Passino, "A class of attractions/repulsion functions for stable swarm aggregations," *International Journal of Control*, vol. 77, no. 18, pp. 1567–1579, 2004.
- [36] —, "Stability analysis of swarms," *IEEE transactions on automatic control*, vol. 48, no. 4, pp. 692–697, 2003.
- [37] —, "Stability analysis of social foraging swarms," *IEEE Transactions on Systems, Man, and Cybernetics, Part B (Cybernetics)*, vol. 34, no. 1, pp. 539–557, 2004.
- [38] V. Gazi, "On lagrangian dynamics based modeling of swarm behavior," *Physica D: Nonlinear Phenomena*, vol. 260, pp. 159–175, 2013.
- [39] T. R. Metcalf, "Resolving the 180-degree ambiguity in vector magnetic field measurements: The 'minimum' energy solution," *Solar Physics*, vol. 155, pp. 235–242, 1994.
- [40] M. Danilova, P. Dvurechensky, A. Gasnikov, E. Gorbunov, S. Guminov, D. Kamzolov, and I. Shibaev, "Recent theoretical advances in non-convex optimization," in *High-Dimensional Optimization and Probability: With a View Towards Data Science*. Springer, 2022, pp. 79–163.
- [41] J. A. Snyman, D. N. Wilke et al., *Practical mathematical optimization*. Springer, 2005.
- [42] M. Frank and P. Wolfe, "An algorithm for quadratic programming," *Naval research logistics quarterly*, vol. 3, no. 1-2, pp. 95–110, 1956.
- [43] "Standard test method for open-hole tensile strength of polymer matrix composite laminates," American Society for Testing and Materials, Tech. Rep. D5766/D5766M – 23, 2023.
- [44] P. Virtanen, R. Gommers, T. E. Oliphant, M. Haberland, T. Reddy, D. Cournapeau, E. Burovski, P. Peterson, W. Weckesser, J. Bright, S. J. van der Walt, M. Brett, J. Wilson, K. J. Millman, N. Mayorov, A. R. J. Nelson, E. Jones, R. Kern, E. Larson, C. J. Carey, Í. Polat, Y. Feng, E. W. Moore, J. VanderPlas, D. Laxalde, J. Perktold, R. Cimman, I. Henriksen, E. A. Quintero, C. R. Harris, A. M. Archibald, A. H. Ribeiro, F. Pedregosa, P. van Mulbregt, and SciPy 1.0 Contributors, "SciPy 1.0: Fundamental Algorithms for Scientific Computing in Python," *Nature Methods*, vol. 17, pp. 261–272, 2020.
- [45] C. R. Harris, K. J. Millman, S. J. van der Walt, R. Gommers, P. Virtanen, D. Cournapeau, E. Wieser, J. Taylor, S. Berg, N. J. Smith, R. Kern, M. Picus, S. Hoyer, M. H. van Kerkwijk, M. Brett, A. Haldane, J. F. del Río, M. Wiebe, P. Peterson, P. Gérard-Marchant, K. Sheppard, T. Reddy, W. Weckesser, H. Abbasi, C. Gohlke, and T. E. Oliphant, "Array programming with NumPy," *Nature*, vol. 585, no. 7825, pp. 357–362, Sep. 2020. [Online]. Available: <https://doi.org/10.1038/s41586-020-2649-2>
- [46] J. A. E. Andersson, J. Gillis, G. Horn, J. B. Rawlings, and M. Diehl, "CasADi – A software framework for nonlinear optimization and optimal control," *Mathematical Programming Computation*, 2018.
- [47] B. Stellato, G. Banjac, P. Goulart, A. Bemporad, and S. Boyd, "OSQP: an operator splitting solver for quadratic programs," *Mathematical Programming Computation*, vol. 12, no. 4, pp. 637–672, 2020. [Online]. Available: <https://doi.org/10.1007/s12532-020-00179-2>
- [48] "Prusaslicer 2.7.2," https://www.prusa3d.com/en/page/prusaslicer_424/, 2024, (Released on 29/02/2024).



optimization, control, and machine learning, with applications to robotic and industrial systems.

XAVIER GUIDETTI received a B.Sc. degree, in 2017, and a M.Sc. degree, in 2019, in mechanical engineering with a major in control and mechatronics from EPFL, Lausanne, Switzerland. He has joined the Automatic Control Laboratory at ETH Zurich in 2019, and is currently a Ph.D. candidate. Concurrently, he is part of the Control and Automation group at inspire AG, a technology transfer center and strategic partner of ETH Zurich. His research interests include data-driven



group at inspire AG, a technology transfer center and strategic partner of ETH Zurich. He is also a guest Senior Scientist at IfA. His research interests include control theory, optimization, statistical learning, robotics, cyber-physical systems, and additive manufacturing.

EFE C. BALTA received a B.S. degree in manufacturing engineering from the Faculty of Mechanical Engineering, Istanbul Technical University, in 2016, and the M.S. and Ph.D. degrees in mechanical engineering from the University of Michigan, Ann Arbor, MI, USA, in 2018 and 2021, respectively. He was a Post-Doctoral Researcher with the Automatic Control Laboratory (IfA), ETH Zurich between 2021 and 2023. Since September 2023, he has been leading the Control and Automation



serving as the Professor for Computation and Control and the Head of the laboratory. His research interests include modelling, analysis, and control of large scale systems, with applications to energy systems, transportation, and industrial processes.

JOHN LYGEROS received a B.Eng. degree in 1990 and an M.Sc. degree in 1991 from Imperial College, London, U.K. and a Ph.D. degree in 1996 at the University of California, Berkeley. After research appointments at M.I.T. and U.C. Berkeley, he joined the University of Cambridge in 2000 as a University Lecturer, and then the University of Patras, Greece, in 2003 as an Assistant Professor. In July 2006 he joined the Automatic Control Laboratory at ETH Zurich where he is currently

...